REPORT VOLCANICA

Effusive pulse at El Reventador volcano, October 2025: andesitic lava flow and lava front collapse-induced pyroclastic density currents

Benjamin Bernard *[α], Marco Almeida[α], Henry Calderón[α], Marco D. Córdova[α], Alicia Guevara[β], Stephen Hernandez[α], Silvana Hidalgo[α], Daniel Pacheco[α], Evelyn Rodriguez[α], Mario Ruiz[α], Daniel Sierra[α], Edwin Telenchana[α], Silvia Vallejo[α], Freddy Vásconez[α], and Francisco J. Vasconez[α]

[α] Instituto Geofísico de la Escuela Politécnica Nacional (IG-EPN), Quito, Ecuador.
[β] Departamento de Metalurgia Extractiva de la Escuela Politécnica Nacional (DEMEX-EPN), Quito, Ecuador.

Submitted: 2026-01-24 | Accepted: 2026-07-13 | Published: 2026-08-02

Editor: E. Gaunt | Production: G. Lerner; J. Farquharson

Abstract

El Reventador, one of Ecuador's most active volcanoes, has experienced near-continuous eruptive activity since 2002. In 2025, beginning on 3 October, summit explosive activity declined sharply. On 6 October, continuous gas emissions increased and a lava flow from the east-southeast vent began advancing. Over the following days, SO_2 emissions were detected by satellite, while the summit explosion rate and seismic noise plummeted. On 12 October, a prolonged collapse of the lava flow front triggered pyroclastic density currents (PDCs) with runouts of up to 2.25 km, the longest observed at the volcano since 2017. The effusive pulse, which produced approximately 2.8–3.2 million m^3 of andesitic lava, ended by 28 October, when explosive activity resumed. This episode highlighted the importance of multiparametric monitoring and targeted fieldwork to track eruptive transitions, reconstruct eruption dynamics, and improve hazard assessment and early warning in remote volcanic regions.

Resumen

El Reventador, uno de los volcanes más activos del Ecuador, ha experimentado una actividad eruptiva casi continua desde 2002. En 2025, a partir del 3 de octubre, la actividad explosiva en la cumbre disminuyó de manera abrupta. El 6 de octubre, las emisiones continuas de gases aumentaron y un flujo de lava comenzó a avanzar desde el vento este-sureste. En los días siguientes, las emisiones de SO_2 fueron detectadas por satélite, mientras que la tasa de explosiones en la cumbre y el ruido sísmico disminuyeron drásticamente. El 12 de octubre, un colapso prolongado del frente del flujo de lava generó corrientes de densidad piroclástica (CDP) con recorridos de hasta 2,25 km, los más largos observados en el volcán desde 2017. El pulso efusivo, que produjo aproximadamente 2,8–3,2 millones de m^3 de lava andesítica, finalizó el 28 de octubre, cuando la actividad explosiva se reanudó. Este episodio destacó la importancia del monitoreo multiparamétrico y del trabajo de campo dirigido para seguir las transiciones eruptivas, reconstruir la dinámica eruptiva y mejorar la evaluación de peligros y la alerta temprana en regiones volcánicas remotas.

Keywords: Volcano monitoring; Field volcanology; Seismic tremor; SO2; Photogrammetry; Mineralogy.

1 Introduction

El Reventador (~3570 m a.s.l.), one of the Ecuador's most active stratovolcanoes, lies in the Subandean zone of the Ecuadorian Andes, about 90 km east of Quito. It is situated within a 4 km × 6 km horseshoe-shaped landslide scar of the ancient Paleo-Reventador volcano (Figure 1). After 26 years of quiescence, El Reventador erupted on 3 November 2002, producing one of Ecuador's largest eruptions in the past century (VEI 4), with significant economic impacts, including road and pipeline disruptions and temporary closure of Quito's airport [Hall et al. 2004].

Since 2002, the volcano has maintained almost continuous activity, characterized by variable eruptive styles, frequent explosions, lava flows, pyroclastic density currents (PDCs), and ash columns reaching up to several kilometers above the crater [Almeida et al. 2019; Gaunt et al. 2024; Hidalgo et al. 2024; Vallejo et al. 2024]. Over the past decade, surface activity levels, according to the IG-EPN monitoring, have ranged from moderate (impact of volcanic phenomena limited to the summit area) to high (impact of volcanic phenomena up to the foot of the cone). During this period, the 22 June 2017 PDCs formed by the collapse of the northeastern border of the summit area reached 3.5 km from the crater, becoming the largest PDC since 2002 [Vallejo et al. 2024].

In October 2025, El Reventador experienced an increase in activity that generated a small lava flow and associated PDCs. This report documents this recent eruptive pulse by integrating multiparametric data from the 24/365 monitoring network with field observations from several campaigns, including drone surveys and deposit sampling.

2 Data and Methods

2.1 Monitoring Network

The activity of El Reventador is monitored by a ground-based network that includes three broadband seismic stations, two of them are coupled with infrasound sensors, two visible cameras, one visible camera trap (one image every 5 minutes without transmission), one thermal camera, one DOAS, and one ultraviolet camera (modified from Hidalgo et al. [2024]; Fig-

* bbernard@igepn.edu.ec

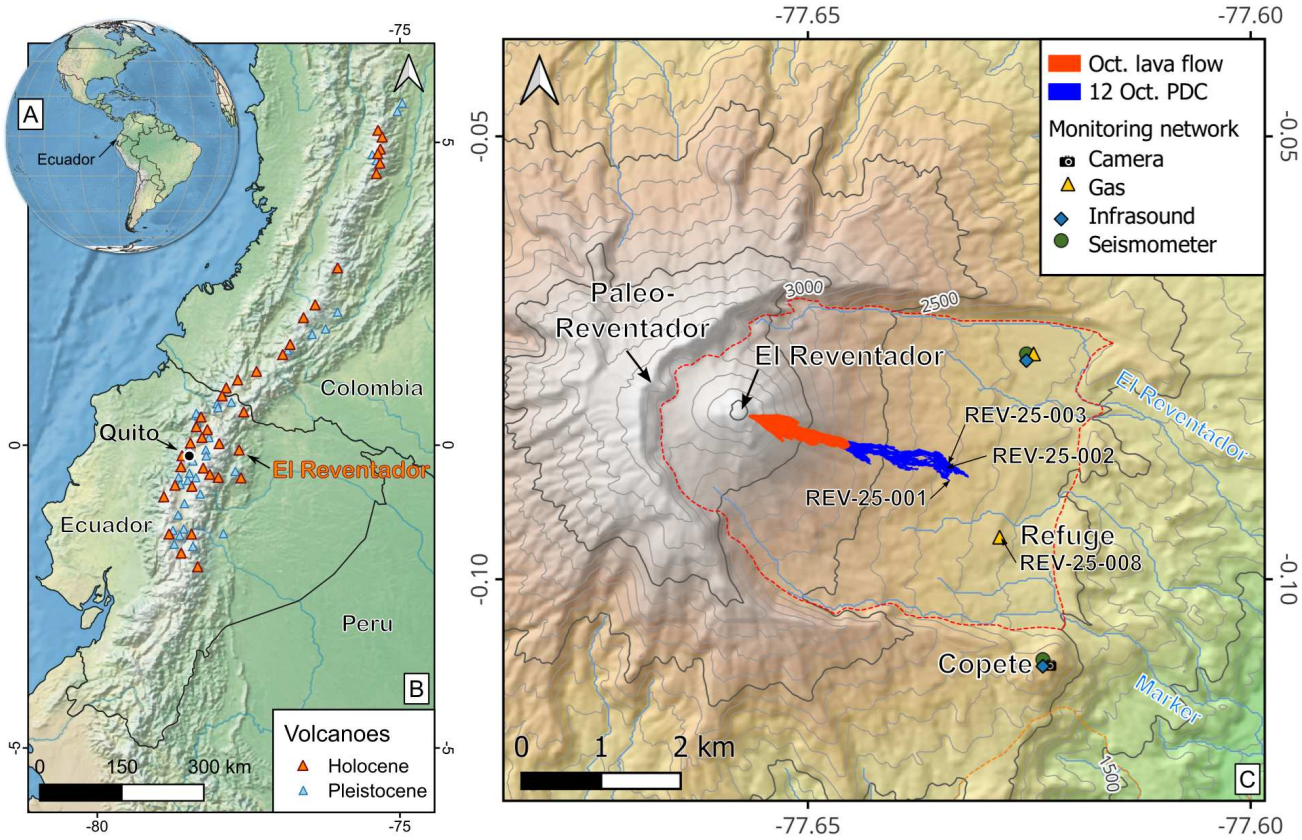


Figure 1: Location of El Reventador volcano. A: Orthographic worldview centered on Ecuador. B: Map of the Northern Volcanic Zone of the Andes. Base map: Natural Earth 1:10 M (https://www.naturalearthdata.com/); Quaternary volcanoes: [Global Volcanism Program 2023]. C: Map of El Reventador volcano, its monitoring network, October 2025 deposit and samples. Red dotted line: limits of El Reventador youngest edifice. Base map: Copernicus Global DSM 30 m.

ure 1C). In addition, satellite sensors (ABI, TROPOMI, VIIRS, MODIS, and SAR) provide data on gas and ash emissions, thermal anomalies, and ground deformation. For this report, the daily explosion rate (Figure 2A) of medium-sized explosions before and after the onset of the effusive pulse is quantified using a catalog derived from a regional seismic network as described in Gaunt et al. [2024], while seismic analysis of significant activity (e.g. Seismic tremor due to PDCs) is described using the local seismic network (Figure 1C and Figure 2B). SO_2 mass (Figure 2C) is derived from the MOUNTS system* using the TROPOMI sensor on board the Sentinel 5 satellite [Valade et al. 2019]. Ash column heights (Figure 2D) are obtained from IG-EPN volcanic observatory notices for aviation (VONAs) based on imagery from the Copete monitoring camera and analysis of GOES-19 satellite data [Vásconez Müller et al. 2024]. Lava flow length (Figure 2E) was monitored using day- and night-time images from the Copete monitoring camera (one image every ~150 s with real-time transmission) and corresponding calibrated overlay†. The plume height overlay was calibrated using trigonometry [Bernard 2018], whereas the overlay for the lava flows, PDCs, and rock falls was drawn by projecting Copernicus 30 m digital surface model (DSM) onto the volcano profile.

*http://mounts-project.com/
†https://www.igepn.edu.ec/reventador-camaras

2.2 Field Campaigns

Two field campaigns (14–16 October and 12–14 November 2025) and one aerial overflight (23 October 2025) were conducted to characterize the October deposits, including lava flows, PDCs, and minor ashfall. Field observations were complemented by UAV surveys (DJI Mavic 3T and DJI Mavic 3M), handheld visible (Sony α7IV) and thermal (FLIR T1020) imagery, and sample collection for laboratory analyses. Lava blocks were collected from the PDC deposits on 15 October, and a small ash-fall sample was gathered from the solar panels of the monitoring station at the Refuge the same day (Figure 1). UAV surveys were conducted using Real-Time Kinematics (RTK) antennas to improve aircraft positioning accuracy. All UAV surveys were conducted from the Refuge (Figure 1). Point clouds, DSMs, and orthomosaics (visible and infrared) were generated using Structure-from-Motion techniques in `Agisoft Metashape Professional v1.5.0`. Thermal images are converted to RGB during photogrammetric processing, which results in the loss of temperature information; therefore, the resulting thermal orthomosaics are used for cartographic purposes only. Visible point clouds were co-registered in `CloudCompare v2.14`, achieving an RMS error of <1 m, and exported as rasters to calculate altitude differences. Raster overlays, calculations, and cartographic products were produced in `QGIS v3.40.6`. Data from a previous UAV survey

(7 April 2025) were also used for comparison with the October and November datasets.

2.3 Laboratory analysis

Semi-quantitative mineralogical analyses on a milled lava block subsample were performed by X-ray diffraction using a Bruker D8 Advance diffractometer and processed with `Diffrac Plus` software at DEMEX-EPN. Thin sections of the same lava block were prepared at the Mineralogy and Petrography Laboratory of the Instituto de Investigación Geológico y Energético (IIGE) and described using a Zeiss Axio Scope A1 microscope at the IG-EPN laboratory. Lava block densities were measured using the Archimedes principle on parafilm-coated samples to determine bulk density, while water pycnometry on milled samples was used to calculate the dense rock equivalent (DRE). Grain-size distributions of the ashfall deposits were obtained through sieving (in half-ϕ intervals down to 4 ϕ or 63 µm) and laser diffraction analyses using a Horiba Partica LA-960 particle size analyzer at the IG-EPN laboratory. The sieving and laser diffraction results were merged at 90 µm (3.5 ϕ). Semi-quantitative component analysis of the 180–250 µm (2.5 ϕ) size fraction was performed by manually classifying 100 particles under a binocular microscope based on their optical, textural and morphological characteristics.

3 Results

3.1 Chronology of the effusive pulse

Prior to the onset of the effusive pulse in October 2025, El Reventador's activity consisted mainly of frequent moderate-size explosions (60–80 per day) from the two summit craters (northwest and southeast), producing ash columns that typically rose 600–2000 m above the summit. In the months leading up to the effusive episode, TROPOMI sensor detected SO_2 only sporadically and in low amounts (<10 tons). Short lava flows (<1 km from the vent) emitted from an effusive vent on the east-southeast flank generated recurrent rockfalls. Although less frequent, small PDCs (<2 km from the summit) produced by either fallback from explosions or collapses of lava flow fronts also contributed to the overall high level of activity [IG-EPN 2023; 2024a; b; c; Crespo Solís 2025].

3.1.1 *Decrease of explosive activity*

On 3–4 October 2025 (① in Figure 2A), a noticeable decrease in the number of daily medium-sized explosions was observed on the regional seismic network as well as at SAG1 infrasound array located 240 km to the south of El Reventador (not shown). This decline in explosive activity coincided with a reduction in seismic noise between 2 and 5 Hz registered in the local seismic network (① in Figure 2B), while the lava flow length (~350 m from the vent) and ash column height (~1000 m above the summit) remained unchanged until 6 October [IG-EPN 2025a].

3.1.2 *Increase of gas emissions and lava flow advance*

Between 6 and 7 October, the gas emission column became noticeably stronger and more continuous. Early on 7 October (② in Figure 2), the lava front began to advance at an average velocity of 6 $m\,hr^{-1}$ (maximum 18 $m\,hr^{-1}$), and by 8 October it had extended to approximately 535 m (Figure 2E). TROPOMI detected low SO_2 emissions on 8 October (10.3 tons), which increased tenfold on 9 October (115.8 tons) and peaked on 11 October (265.5 tons, the highest value registered in the last two years; ③ in Figure 2C). Associated with the increase in gas emission, ash column height reached ~1500 m above the summit (Figure 2D). The lava front continued advancing, although more slowly (~ 1.2 $m\,hr^{-1}$), until 12 October, a period during which the number of explosions dropped to a minimum (<10 per day). Frequent small collapses from the front and flanks of the lava flow occurred throughout this period (Figure 3A).

3.1.3 *Lava flow front collapse and pyroclastic density currents*

On 12 October at 18:19:10 local time, a 50-minute tremor of variable amplitude was recorded [IG-EPN 2025a] (Figure 4), coinciding with the collapse of the lava flow front and the generation of PDCs on the eastern flank (④ in Figure 2). Surveillance imagery indicates that the first small PDC was observed by the Copete camera at ~18:19, followed by the development of a co-PDC ash cloud at ~18:22. The camera trap located near the refuge recorded the first PDC at ~18:20 (Figure 3B) and the associated ash cloud at ~18:25 (Figure 3C). The PDCs eroded a gully on the volcano's flank (Figure 3D; Figure 5H). This event generated minor ashfall in the immediate surroundings of El Reventador (Hostería El Reventador, San Carlos, and Piedra Fina), likely related to the co-PDC ash cloud, which rose to approximately 2300 m above the summit and drifted southward. Plume height was estimated from satellite data, as the Copete camera was completely obscured by ash during the event. According to surveillance camera imagery and seismo-acoustic signals, the episode was not accompanied by an explosive eruption [IG-EPN 2025a]. After the collapse, lava effusion continued and the flow front advanced at an increased rate of ~2.2 $m\,hr^{-1}$ until 16 October (Figure 5D, 5E).

3.1.4 *Decline of the effusive pulse*

In the following weeks, the lava flow continued to progress, accompanied by nearly continuous rockfall activity (Figure 5B). By 28 October, the flow extended ~1300 meters before its progression largely halted (Figure 5H and 5G). Overall, the lava advanced at an average rate of 1.6 $m\,hr^{-1}$ (38 m per day, linear regression in Figure 2D) between 6 and 28 October. Following the collapse event, SO_2 emissions dropped to low levels (<10 tons; ⑤ in Figure 2), though intermittent gas releases persisted into November. Meanwhile, the level of explosive activity gradually increased (Figure 5A), reaching approximately 35 explosions per day when the lava flow stopped (⑥ in Figure 2). Concurrently, ash emissions intensified: by early November, several eruption columns exceeded 2000 m in height (⑦ in Figure 2). Ashfall events became more frequently reported, likely influenced by both higher plume altitudes and shifting wind patterns associated with the seasonal "veranillo" phenomenon, typical of November–December in Ecuador.

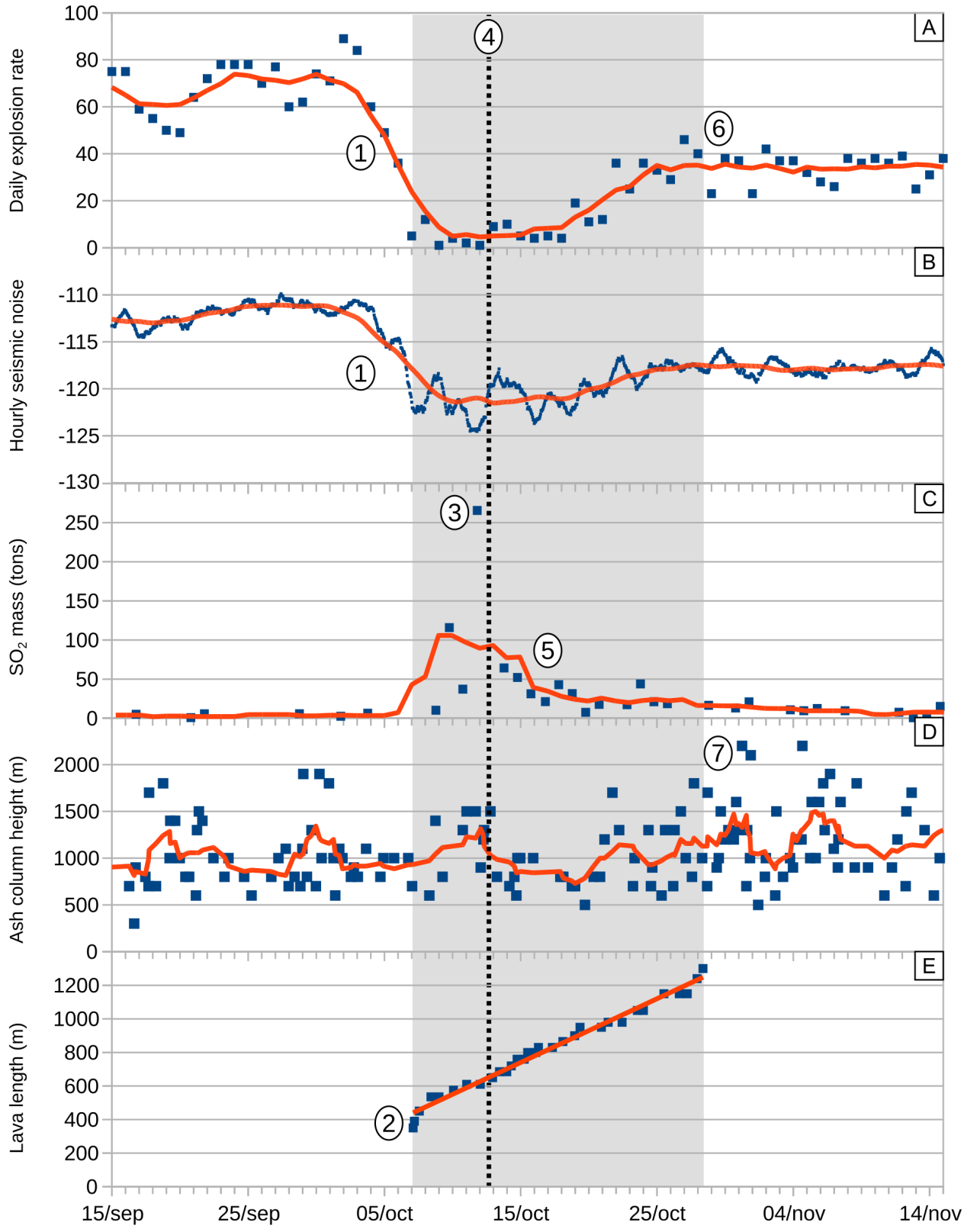


Figure 2: Multiparametric evolution of activity at El Reventador from 15 September to 14 November 2025. Blue squares denote individual measurements, and red lines indicate a 7-point moving average, except for the lava length where it represents a linear regression and for the seismic noise where it represents a 7-day average. The vertical dotted line marks the timing of the 12 October PDCs; the gray shaded area highlights the period of lava flow advance, and numbers ①–⑦ refer to events discussed in the text.

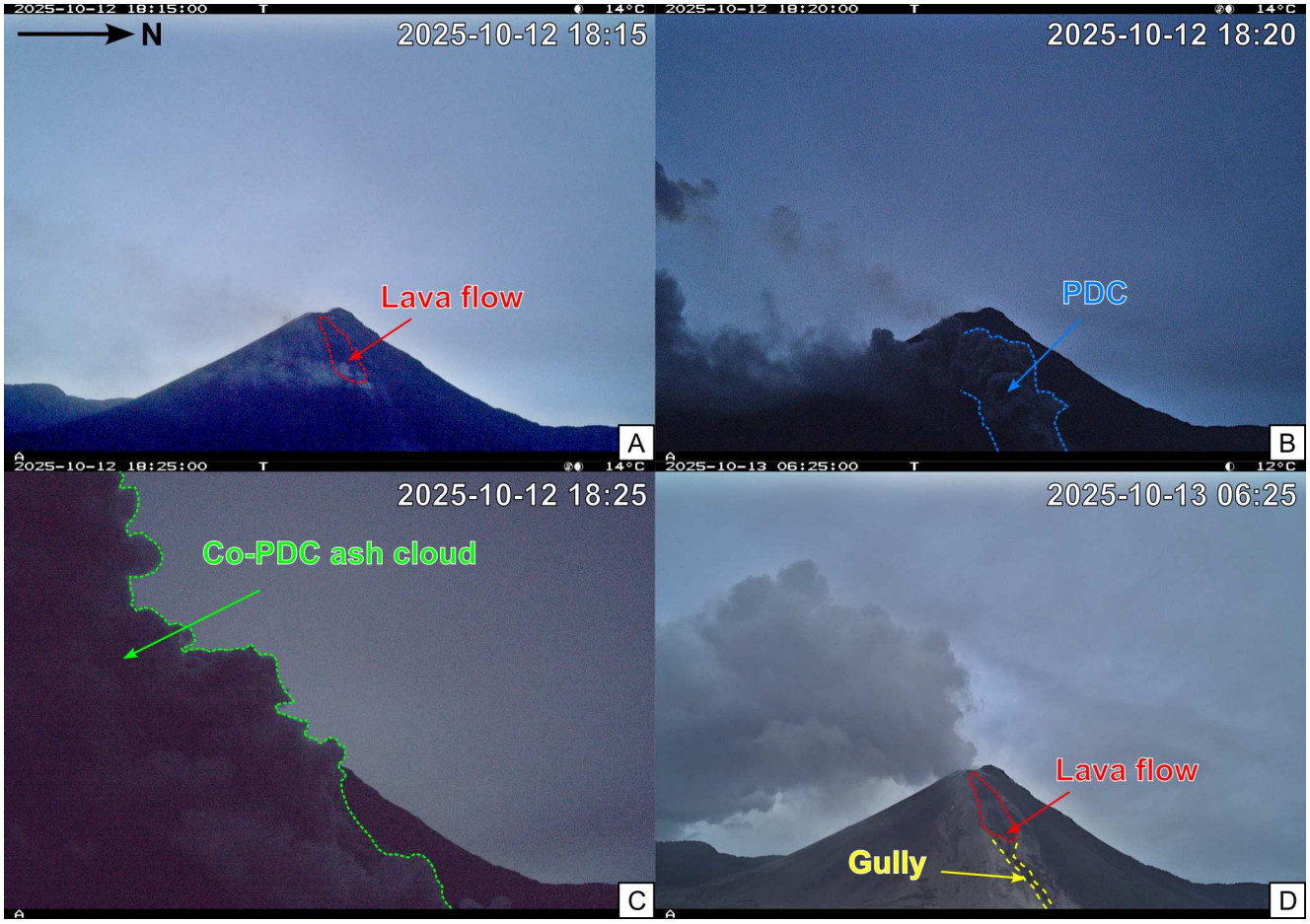


Figure 3: Photographs from the camera trap located at the Refuge. [A]: Start of the collapse of the lava flow on 12 October. [B]–[C]: pyroclastic density current due to the collapse of the lava flow front. [D] Gully formation as an erosive process due to the PDC.

3.2 Mapping and characterization of the new deposits

3.2.1 *Lava flow*

Using UAV imagery (both visible and infrared) acquired during the field campaigns, two maps of the advancing lava flow were produced and compared with a previous map from April 2025 (Figure 6A, 6B, and 6C). Comparison of the aligned DSMs from 7 April, 15 October, and 13 November 2025 allowed us to accurately estimate the thickness and volume of the new deposits (Figure 6D and 6E). During both drone surveys, the maximum lava temperature exceeded 500 °C, corresponding to the upper measurement limit of the Mavic 3T thermal sensor operating in Low Gain Mode. Measurements with a FLIR T1010 handheld thermal camera from the Refuge on 15 October yielded a maximum temperature of 557 °C.

On 15 October, the lava flow extended 732 m in length (4 % shorter than the estimate from the Copete monitoring camera), reached a maximum width of 250 m, and covered an area of 0.124 km^2 (Figure 6B). Subtracting the October and April DSMs yields an average lava thickness of 12.7 m, with a maximum of 28.4 m, corresponding to a total volume of 1.58 million m^3 (Figure 5D). While the mapped area closely matches the preliminary estimate reported in the early-November special report [IG-EPN 2025b], the calculated volume is ~40 % larger. This difference reflects the inclusion of April topography in our analysis. Accordingly, the special report volume (1.13 million m^3), which assumes a flat basal surface, represents a minimum, whereas our estimate should be regarded as a maximum, as material emplaced between April and October (e.g. PDC and rockfall deposits) may be included. For this period (6–15 October), the Time-Averaged Discharge Rate (TADR) is estimated between 1.5 and 2.0 m^3 s^{-1}.

By 13 November, the lava flow had advanced to 1325 m in length (2 % longer than the Copete camera estimate), expanded to 305 m in width, and covered an area of 0.224 km^2 (Figure 6C). The DSM difference between November and April shows a mean thickness of 16.3 m and a maximum of 41.7 m, yielding a total volume of 3.65 million m^3. As before, this value likely represents an upper bound because it includes pyroclastic deposits emplaced during the April–October period (Figure 6 and Figure 7). If lava advance ceased around 28 October, the volume increase of 1.64 million m^3 (Figure 6E) corresponds to a TADR of ~1.5 m^3 s^{-1}. In addition to the advance of the lava field, a new lobe developed north of the main flow, and a central lava channel formed above a gully previously carved by the 12 October PDCs (Figure 7).

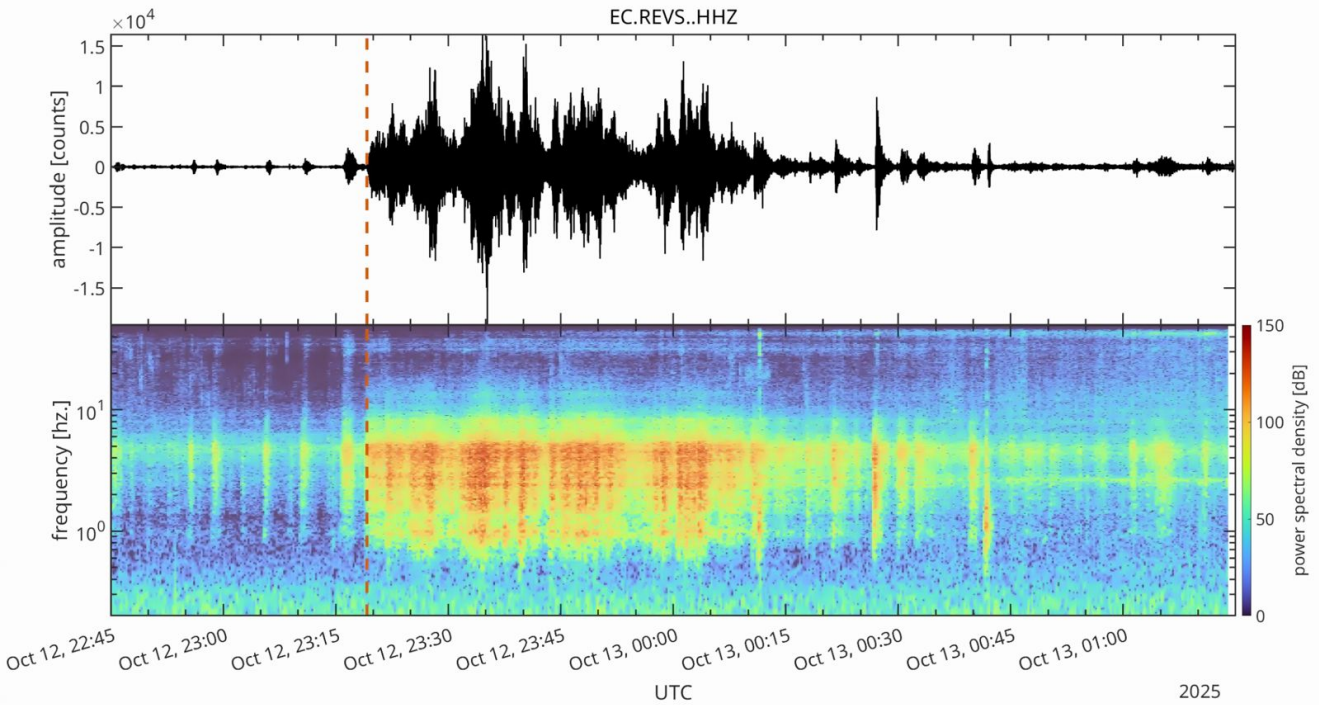


Figure 4: Seismic signal produced by the 12 October 2025 PDCs. (Top) REVS broadband data, high-pass filtered at 0.2 Hz. (Bottom) Spectrogram representing the power spectral density (in dB) as a function of frequency and time. The red dashed lines (23:19 UTC) indicate the estimated start of the continuous tremor sequence.

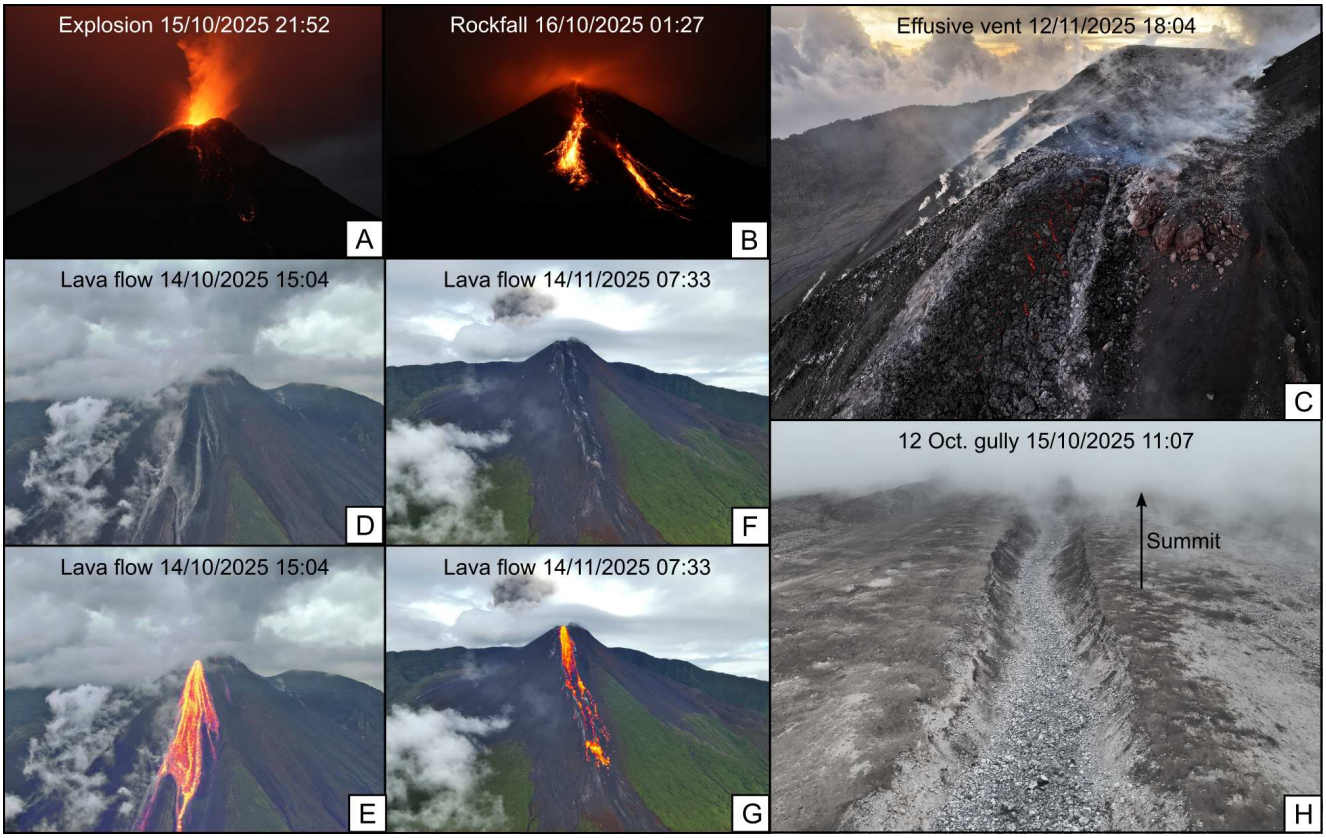


Figure 5: Photographs of the activity and features observed at El Reventador volcano between October and November 2025 (local time). [A] Typical low energy explosive activity; [B] Rockfall from the active lava flow; [C] Aerial view of the east-southeast vent; [D] and [E] Aerial view of the lava flow on 14 October with overlaid thermal image; [F] and [G] Aerial view of the lava flow on 14 November with overlaid thermal image; [H] Aerial view of the gully carved by the 12 October PDCs.

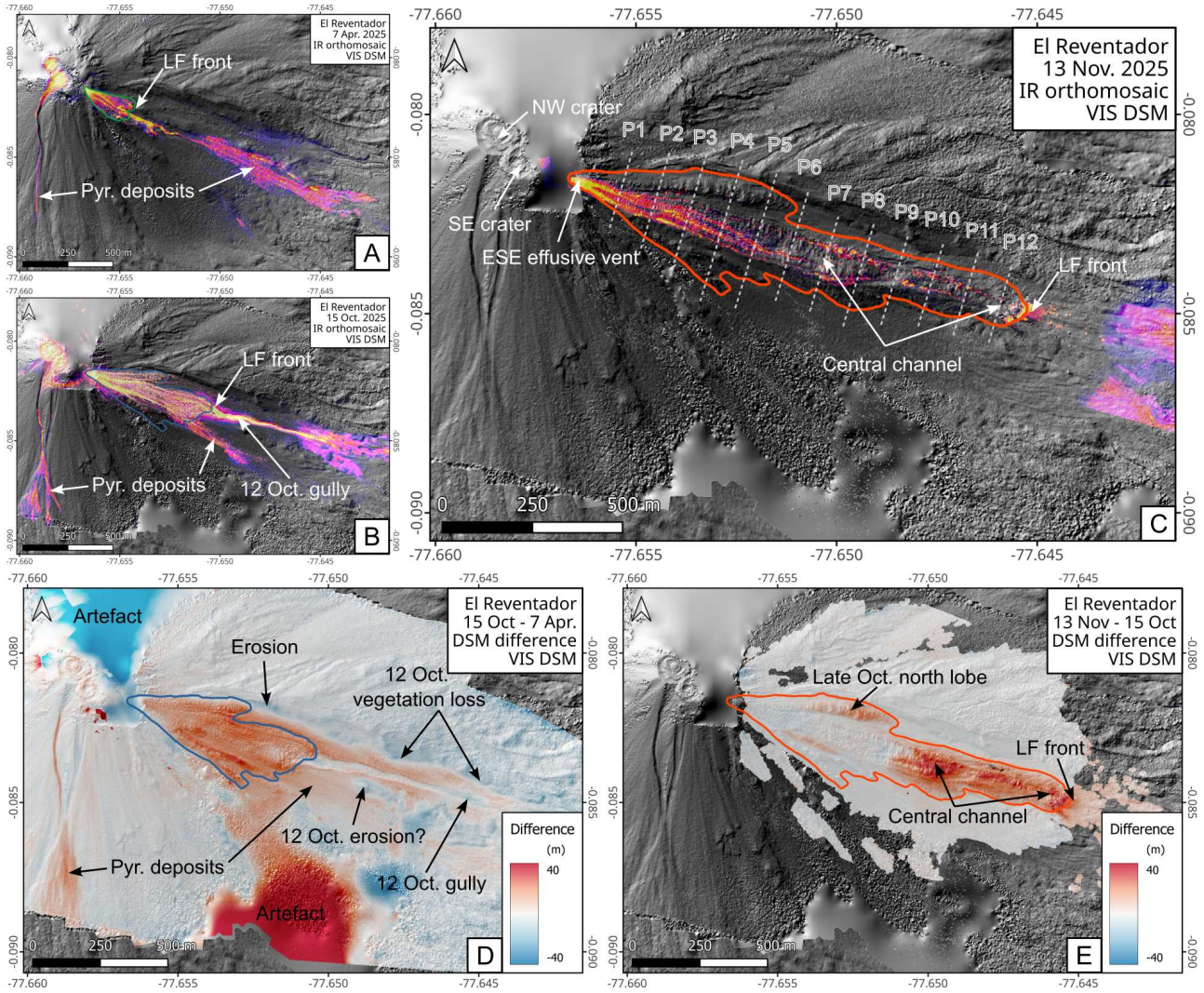


Figure 6: Maps of the recent effusive activity at El Reventador volcano. [A], [B], and [C] correspond to infrared orthomosaics overlaid on visible DSMs. [D] and [E] correspond to DSM differences between visible DSMs. LF: lava flow; Pyr.: pyroclastic; P1-12: topographic profiles represented in Figure 7.

3.2.2 *Pyroclastic density currents*

The 12 October PDCs travelled approximately 2250 m from the lava front, descending ~770 m in elevation (H/L = 0.34) and covering an area of 0.25 km^2 (Figure 8). The PDCs came to a halt approximately 850 m northwest of the Refuge, traveling within a drainage that feeds the Reventador River (Figure 1C). Estimation of deposit volume using DSM differencing was not feasible, as the PDCs entered a densely vegetated zone. Tree removal in the medial and distal sectors produced negative elevation changes, whereas pre-existing April–October pyroclastic deposits led to overestimation in the proximal area. Nevertheless, local measurements using DSM differencing within the main drainage followed by the PDCs indicate deposit thicknesses of up to 6 m. The presence of kipukas within the PDC deposits (Figure 8A and 8B) indicates that the currents were relatively thin. The PDCs carved a gully over 630 m long, up to 40 m wide, and as much as 10 m deep within what is likely a recent debris fan composed mainly of pyroclastic deposits emplaced between June 2024 and October 2025 (Figure 6, 7, and 8).

A field survey conducted on 15 October revealed deposits composed of lava blocks embedded in an ash-rich matrix. Three days after emplacement, block surface temperatures remained as high as 370 °C, while the ground was still 50–60 °C. The PDC front visited in the field was approximately 1.5 m thick (Figure 8C). Based on these observations and the maximum thickness measured in the main drainage, the average deposit thickness ranges between 1.5 and 3 m, corresponding to a total volume of approximately 0.37–0.75 million m^3.

Lava block samples were analyzed in laboratory and identified as dense andesite (bulk density 2525–2526 kg m^{-3}, DRE 2674–2678 kg m^{-3} DRE, ~6 vol.% vesicularity). The andesite contains phenocrysts of plagioclase, orthopyroxene, clinopyroxene (augite), olivine, magnetite, and trace amphibole (hornblende) with a microcrystalline matrix (Figure 9).

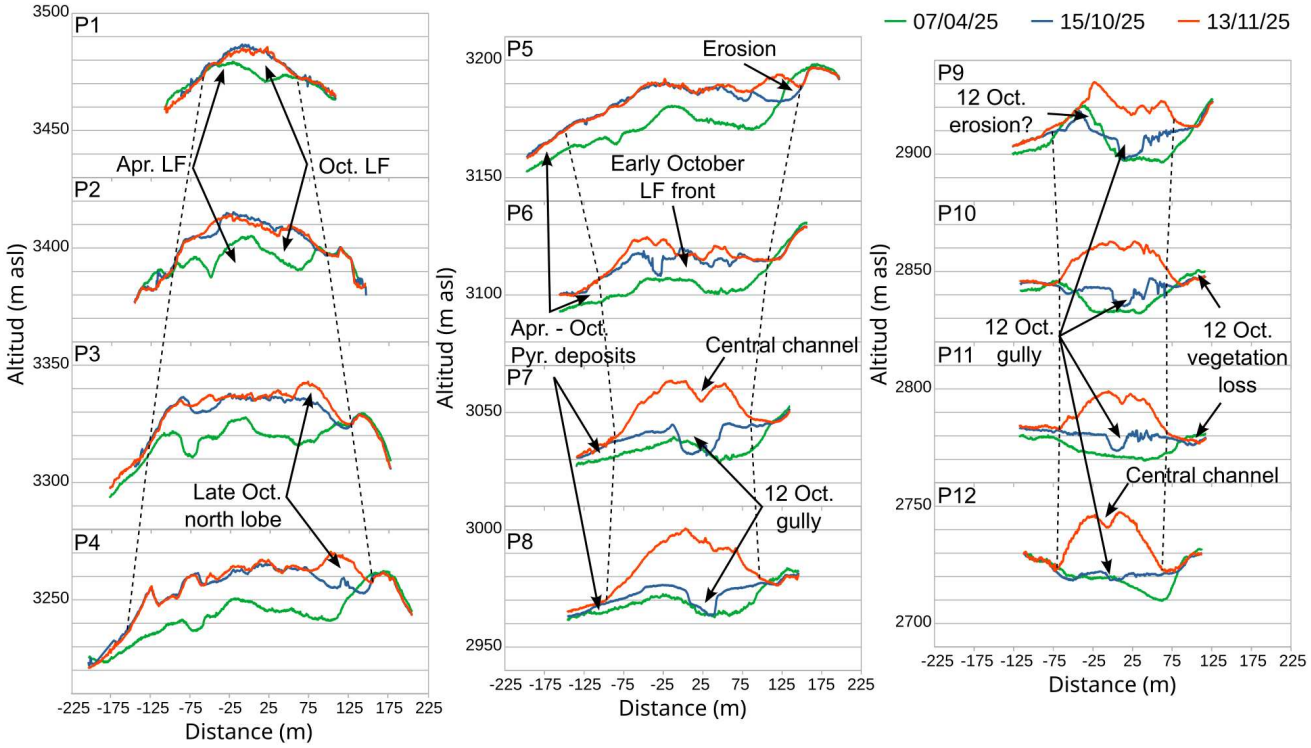


Figure 7: Topographic profiles of the October lava flow with superposition of the April (green), October (blue), and November (red) topography. LF: lava flow; Pyr.: pyroclastic; P1-12: topographic profiles located in Figure 4.

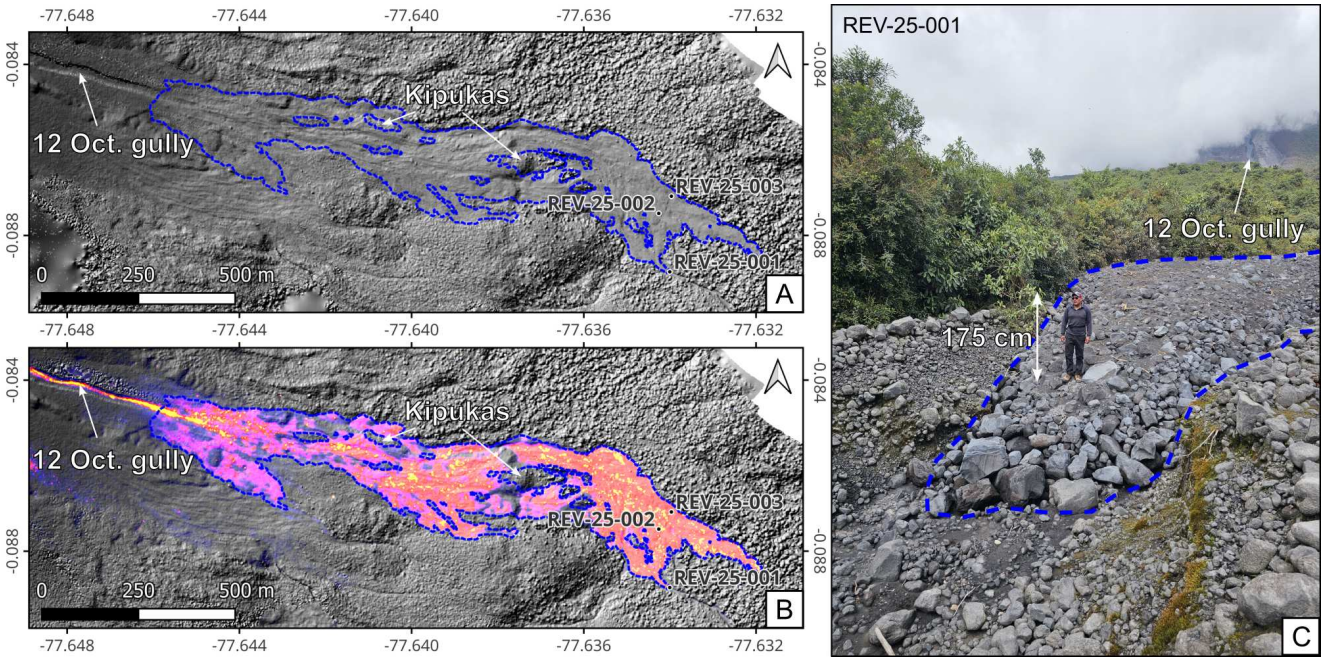


Figure 8: Maps and photograph of the PDC deposits. A: 15 October DSM and B: 15 October DSM combined with infrared orthomosaics acquired on 14 October. C: Photograph of the PDC deposit front at site REV-25-001.

3.2.3 *Ash fallout*

During the night of 14–15 October, a very minor ash fall occurred at the Refuge (Figure 1C), with an accumulated load of 2.4 $g\,m^{-2}$. The deposit is fine grained (mean = 3.52 ϕ), poorly sorted (standard deviation = 1.14 ϕ), strongly positively skewed (skewness = 1.65 ϕ), and leptokurtic (kurtosis = 2.09 ϕ). The distribution exhibits a dominant fine mode at 2.85 ϕ and a secondary, extremely fine mode at 4.92 ϕ (Figure 10A), which is probably the result of sedimentation of ash aggregates [Miwa et al. 2020].

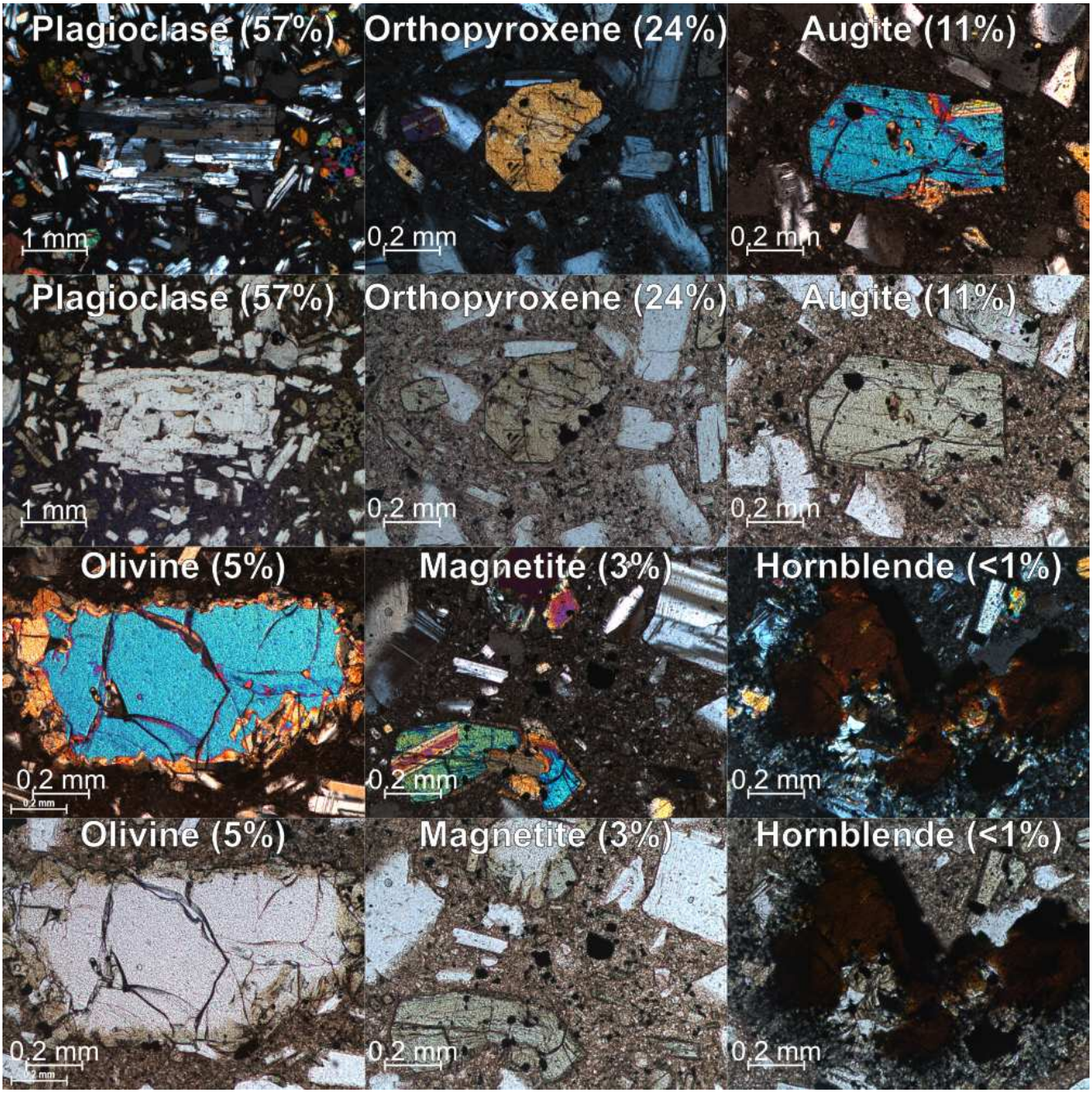


Figure 9: Natural and polarized light microphotographs of the mineral assemblage of the lava block from the REV-25-002c sample. Semi-quantitative proportions were obtained by X-ray diffraction.

Semi-quantitative component analysis of the 180–250 μm (2.5 φ) size fraction reveals a predominance of gray to black particles with a glassy to metallic luster and very low vesicularity (Figure 10B). Only minor amounts of hydrothermally altered or oxidized material and a few free crystals (mostly plagioclase and pyroxene) were observed.

4 Discussion

4.1 Vent location at El Reventador

High-resolution UAV surveys, conducted during and after the effusive pulse, allowed for the accurate mapping of the lava flow source. At El Reventador, most lava effusion, whether forming domes or lava flows, typically originates from the summit craters [Vallejo et al. 2024]. However, the vent responsible for the October eruption (77.65668° W, 0.08154° S; ~3530 m a.s.l.) is situated on the east-southeast flank, roughly 150 meters from the southern summit vent, and first opened in June 2024 [Crespo Solís 2025] (Figure 5C).

Lateral vents have been documented on three occasions before: in 2002 down on the southeast flank [Hall et al. 2004], in 2017 on the north flank close to the summit [Almeida et al. 2019], and in 2018 down on the west flank and at the opening of the 2018 landslide scar [Vallejo et al. 2024]. These vents

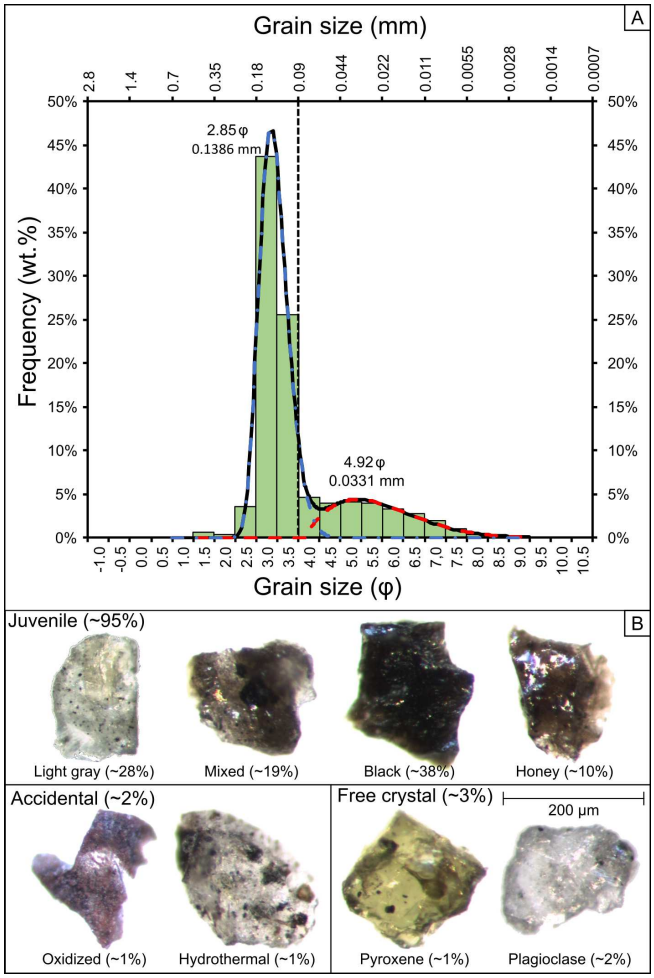


Figure 10: [A] Grainsize distribution and [B] semi-quantitative componentry of REV-25-008 ash sample (180-250 µm fraction) collected on 15 October at El Reventador refuge.

were short-lived (few days to months), quickly shifting activity back to the central summit vents.

The new east-southeast vent, however, is located less than 20 m downslope from the headwall of the 2018 landslide scar [Vallejo et al. 2024] and has remained active for two consecutive years. The shift in lava effusion from the summit craters to this flank vent may be linked to the pyroclastic cone reaching its maximum stable height [Vallejo et al. 2024; Crespo Solís 2025]. This could impede magma ascent to the summit due to increased lithostatic load, combined with structural weaknesses at the contact between the 2018 landslide scar and the overlying pyroclastic cone. Such branching of the conduit feeding system has previously explained the distinct activity of the two summit craters, with the north vent being mostly effusive and the south vent primarily explosive [Gaunt et al. 2024; Vallejo et al. 2024].

4.2 Origin of the effusive pulse and decrease of explosivity

The mineral composition of the lava block closely resembles that of the 2002–2018 eruptions [Galárraga 2022], though with slightly varying proportions, with more orthopyroxene, for example. Amphibole was present in lavas erupted between 2002 and 2008 but was not identified in those emplaced between 2009 and 2018; however, it reappears as an accessory mineral in the October 2025 lava. Additionally, volcanic monitoring detected no significant internal activity, such as deep long-period or volcano-tectonic events immediately before the effusive pulse. In contrast, although the increase in SO_2 emissions is evident, it remains modest compared with the pre-eruptive SO_2 emissions observed at other Ecuadorian andesitic volcanoes, such as Tungurahua and Cotopaxi [Hidalgo et al. 2015; 2018]. The relatively limited SO_2 output at El Reventador may be explained by decompression of a slightly differentiated magma residing in a shallow reservoir and reaching the SO_2 exsolution level, without requiring the intrusion of a large volume of gas-rich magma from greater depth.

The absence of coarse vesicular particles in the 15 October ash fallout aligns with weak explosive activity, characterized by a low eruptive column (<1.2 km [Gaunt et al. 2024]). Grain-size distribution and component analysis suggest fragmentation of a highly crystallized, largely degassed magma, likely driven by decompression in a weak Vulcanian-style eruption [Miwa et al. 2013; Battaglia et al. 2019; Gabellini et al. 2022; Gaunt et al. 2024].

Taken together, the lava-block and ash-sample data suggest that the eruptive pulse was likely triggered by the relatively rapid decompression of a differentiated magma already residing within the conduit. This magma was sufficiently hot to ascend with limited seismicity and had undergone partial degassing, thereby accounting for the low explosivity and relatively high density of the erupted products. The reduced explosivity during the effusive pulse may also originate from the magma's relatively low volatile content and the decrease in internal pressure due to the increased effusive rate. These hypotheses could be further evaluated through detailed geochemical and petrological investigations, as well as comprehensive ground-deformation analyses, which are beyond the scope of this study.

4.3 Quantitative evaluation

From 6 to 28 October, the lava flow advanced to approximately 1325 m, reaching a total volume of around 2.8–3.2 million m^3. This volume is close to the median value reported for lava flows from the 2002–2009 period (3.4 million m^3), although the inferred TADR (~1.5–1.7 $m^3\,s^{-1}$) is considerably lower than the average for that period (7.3 $m^3\,s^{-1}$ [Naranjo et al. 2016]). This difference of TADR could be associated with the higher SiO_2 content of the October 2025 lava compared to the 2002–2009 period [Galárraga 2022]. Both the volume and effusion rate fall at the upper end of the reported ranges for the 2012–2016 period (0.46–8.9 million m^3 and 0.1–2 $m^3\,s^{-1}$, respectively [Arnold et al. 2019]). The June 2024 lava flow (volume: 0.9–1.1 million m^3 [Crespo Solís 2025]), and subsequent flows were substantially smaller than the October 2025 flow. Considering recent activity, this effusive pulse is interpreted as the largest since 2021 [Vallejo et al. 2024].

The 12 October PDCs travelled up to 2250 m from the lava front, descending ~770 m and covering ~0.25 km^2 with roughly 0.37–0.75 million m^3 of material. While short-runout PDCs are common at El Reventador, the scale of this event is

exceptional. In the current eruptive period, only the 3 November 2002 (VEI 4; column collapse [Hall et al. 2004]) and the 22 June 2017 (VEI ~2; crater collapse [Vallejo et al. 2024]) events surpassed it in runout distance and covered area.

Based on the bulk density of the lava block, an estimated density of 1600–2000 kg m^{-3} for the PDC deposits [Pyle 2015], and neglecting the ash fallout that was minor during the effusive pulse, we calculate a total mass of 7.7–9.3 × 10^{9} kg and a Mass Eruptive Rate (MER) of 4032–4884 kg s^{-1} for the October effusive pulse and associate PDCs. This translates to a magnitude of 2.9–3.0 and an intensity of 6.6–6.7 [Pyle 2015].

4.4 Lava flow front collapse and PDCs hazard assessment

Direct observations and deposit characteristics confirm that the PDCs originated from repeated collapses of the lava flow front, similar to the activity observed at Sinabung volcano between 2013 and 2015 [Pallister et al. 2019]. Despite their relatively thin average thickness (1.5–3 meters), these PDCs were erosive enough to carve a deep gully into recent previous pyroclastic deposits, which were later completely covered by the advancing lava flow.

In response to the change in volcanic activity observed starting on 6 October, the IG-EPN monitoring protocols prompted an update of the surface activity level on 8 October, shifting from "High: No change" to "High: Increasing". Local authorities and nearby communities were subsequently informed of the potential for a more intense eruptive event in the following days. This update was formally documented in the Daily Report of El Reventador Volcano No. 2025-281*.

Both the lava flows and PDCs align with the eruptive scenario described in the June 2024 special report [IG-EPN 2024a], which anticipated a typical runout of 2.5 km from the crater area. However, the October 2025 pulse introduced a key difference: the scenario did not account for moderate-runout PDCs forming at the lava flow front, extending the hazard zone by approximately 500 meters (3 km from the crater area). Moving forward, hazard assessments should incorporate the real-time position of the lava flow front to dynamically map the associated hazard zone.

For rapid response, an energy cone approach could be applied, using the H/L ratio (0.34) derived from this study, along with a safety buffer [e.g. Aravena et al. 2024].

5 Conclusions

The October 2025 effusive pulse at El Reventador was characterized by a marked decrease in explosive activity accompanied by a moderate increase in SO_2 emissions, indicating a temporary shift in the eruptive regime. The andesitic lava flow emplaced during this episode reached one of the largest volumes observed in recent years, and both its volume and discharge rate were at the upper end of values reported since 2009, although they remain within the historical range documented at El Reventador. The eruption was fed by a persistent lateral vent on the east-southeast flank that has remained active since 2024 and may reflect a long-term reorganization of magma ascent pathways within the volcanic edifice.

Subsequent collapses of the lava flow front generated PDCs without associated explosions, highlighting the importance of effusive and gravitational processes in hazard generation at El Reventador. Following the cessation of lava advance, explosive activity, seismicity, and ash emissions increased again in early November, suggesting a rapid return to the volcano's more typical mild explosive behavior. These transitions emphasize the highly dynamic nature of activity at El Reventador and the persistent hazards associated with the interaction of effusive, explosive, and collapse-driven processes within an open-vent system.

Overall, this study demonstrates the value of integrating continuous multiparametric monitoring with targeted field observations and UAV-based surveys to better constrain eruptive dynamics, eruption size, quantify lava emplacement, and improve hazard assessment at persistently active volcanoes. The rapid response of the IG-EPN monitoring team during the crisis enabled timely communication with local authorities and stakeholders in the tourism sector, contributing to effective risk management and public safety.

Author Contributions

BB conceived and coordinated the study, conducted fieldwork, prepared the figures, analyzed the data, and drafted the manuscript. MA, ET, and FV contributed to field data collection. HC mapped the deposits on 15 October using visible and thermal orthomosaics and carried out field observations. MC contributed to figure editing. AG performed the XRD analyses. SHe processed seismic data from the regional network, while DP processed seismic data from the local network. SHi contributed to the design of the report. ER prepared and analyzed ash samples, including grain-size distribution and componentry. SV processed handheld thermal imagery and analyzed camera-trap images. FJV processed and analyzed TROPOMI SO_2 data using the MOUNTS platform. MR and DS contributed to manuscript drafting. All authors participated in monitoring data acquisition and reviewed and approved the final manuscript.

Acknowledgements

The authors gratefully acknowledge the owners and staff of Hostería El Reventador for their logistical support during field campaigns. We thank the Secretaría de Gestion de Riesgos and the Ecuadorian Air Force Transport Wing No. 11, particularly the DHC-6 Twin Otter team of Light Transport Squadron No. 1113 "Tucanes," for facilitating the overflight on 23 October 2025. We also acknowledge the personnel of IIGE and DEMEX-EPN for the rapid processing of samples, and we recognize the dedication of the IG-EPN staff who ensure continuous volcanic monitoring on a 24/365 basis. This study, particularly the drone surveys, was conducted within the framework of the PIS-23-11 project, funded by EPN and led by BB. We thank the two anonymous reviewers for their thoughtful and constructive comments, and Elizabeth Gaunt for handling the review process.

*https://www.igepn.edu.ec/servicios/busqueda-informes

Data Availability

The monitoring data supporting this study can be obtained from the authors upon request. Access to point clouds, DSMs, and orthomosaics generated within the PIS-23-11 project is restricted until the end of the project.

Copyright notice

© The Author(s) 2026. This article is distributed under the terms of the Creative Commons Attribution 4.0 International License, which permits unrestricted use, distribution, and reproduction in any medium, provided you give appropriate credit to the original author(s) and the source, provide a link to the Creative Commons license, and indicate if changes were made.

References

Almeida, M., H. Gaunt, and P. Ramón (2019). "Ecuador's El Reventador Volcano Continually Remakes Itself". *Eos* 100. DOI: 10.1029/2019eo117105.

Aravena, A., A. Tadini, A. Bevilacqua, P. Samaniego, B. Bernard, S. Hidalgo, J.-L. Le Pennec, P. Martínez-Yáñez, J. García, and O. Roche (2024). "Probabilistic, scenario-based hazard assessment for pyroclastic density currents at Tungurahua volcano, Ecuador". *Bulletin of Volcanology* 86(10). DOI: 10.1007/s00445-024-01768-y.

Arnold, D., J. Biggs, H. Dietterich, S. Vallejo Vargas, G. Wadge, and P. Mothes (2019). "Lava flow morphology at an erupting andesitic stratovolcano: A satellite perspective on El Reventador, Ecuador". *Journal of Volcanology and Geothermal Research* 372, pages 34–47. DOI: 10.1016/j.jvolgeores.2019.01.009.

Battaglia, J., S. Hidalgo, B. Bernard, A. Steele, S. Arellano, and K. Acuña (2019). "Autopsy of an eruptive phase of Tungurahua volcano (Ecuador) through coupling of seismo-acoustic and SO2 recordings with ash characteristics". *Earth and Planetary Science Letters* 511, pages 223–232. DOI: 10.1016/j.epsl.2019.01.042.

Bernard, B. (2018). "Rapid hazard assessment of volcanic ballistic projectiles using long-exposure photographs: insights from the 2010 eruptions at Tungurahua volcano, Ecuador". *Volcanica* 1(1), pages 49–61. DOI: 10.30909/vol.01.01.4961.

Crespo Solís, V. Y. (2025). *Cambios morfológicos en las cumbres de los volcanes Cotopaxi y El Reventador: relación con su actividad eruptiva reciente*. Quito: Escuela Politécnica Nacional.

Gabellini, P., R. Cioni, N. Geshi, M. Pistolesi, T. Miwa, G. Lacanna, and M. Ripepe (2022). "Eruptive dynamics and fragmentation mechanisms during cyclic Vulcanian activity at Sakurajima volcano (Japan): Insights from ash texture analysis". *Journal of Volcanology and Geothermal Research* 428, page 107582. DOI: 10.1016/j.jvolgeores.2022.107582.

Galárraga, M. (2022). "Changes in eruptive dynamics in long-lasting eruptions of andesitic volcanoes". Master's thesis. Université Clermont Auvergne.

Gaunt, H. E., M. M. Pique, S. Hernández, S. Hidalgo, M. D. Córdova, P. Ramón, and B. Bernard (2024). "Unravelling eruption dynamics at El Reventador, Ecuador: linking the physiochemical properties of volcanic ash with geophysical, geochemical and satellite remote sensing data". *Bulletin of Volcanology* 86(11). DOI: 10.1007/s00445-024-01777-x.

Global Volcanism Program (2023). "Volcanoes of the World (v. 5.1.0; 9 Jun 2023)". Edited by E. Venzke. DOI: 10.5479/si.GVP.VOTW5-2023.5.1. [Dataset].

Hall, M., P. Ramón, P. Mothes, J. L. LePennec, A. García, P. Samaniego, and H. Yepes (2004). "Volcanic eruptions with little warning: the case of Volcán Reventador's Surprise November 3, 2002 Eruption, Ecuador". *Revista geológica de Chile* 31(2). DOI: 10.4067/s0716-02082004000200010.

Hidalgo, S., J. Battaglia, S. Arellano, D. Sierra, B. Bernard, R. Parra, P. Kelly, F. Dinger, C. Barrington, and P. Samaniego (2018). "Evolution of the 2015 Cotopaxi Eruption Revealed by Combined Geochemical and Seismic Observations". *Geochemistry, Geophysics, Geosystems* 19(7), pages 2087–2108. DOI: 10.1029/2018gc007514.

Hidalgo, S., J. Battaglia, S. Arellano, A. Steele, B. Bernard, J. Bourquin, B. Galle, S. Arrais, and F. Vásconez (2015). "SO2 degassing at Tungurahua volcano (Ecuador) between 2007 and 2013: Transition from continuous to episodic activity". *Journal of Volcanology and Geothermal Research* 298, pages 1–14. DOI: 10.1016/j.jvolgeores.2015.03.022.

Hidalgo, S., B. Bernard, P. Mothes, C. Ramos, J. Aguilar, D. Andrade, P. Samaniego, H. Yepes, M. Hall, A. Alvarado, M. Segovia, M. Ruiz, P. Ramón, and M. a. Vaca (2024). "Hazard assessment and monitoring of Ecuadorian volcanoes: challenges and progresses during four decades since IG-EPN foundation". *Bulletin of Volcanology* 86(1). DOI: 10.1007/s00445-023-01685-6.

Instituto Geofísico de la Escuela Politécnica Nacional (2023). "Vigilancia volcánica y estudio geomorfológico en el volcán El Reventador". URL: https://www.igepn.edu.ec/interactuamos-con-usted/2089-vigilancia-volcanica-y-estudio-geomorfologico-en-el-volcan-el-reventador. Accessed 2025-11-26.

– (2024a). "Informe Volcánico Especial – El Reventador". (2024-001). URL: https://www.igepn.edu.ec/interactuamos-con-usted/2089-vigilancia-volcanica-y-estudio-geomorfologico-en-el-volcan-el-reventador. Accessed 2025-11-26.

– (2024b). "Trabajos de mantenimiento y vigilancia en el volcán El Reventador". URL: https://www.igepn.edu.ec/interactuamos-con-usted/2173-trabajos-de-mantenimiento-y-vigilancia-en-el-volcan-el-reventador. Accessed 2025-11-26.

– (2024c). "Trabajos de monitoreo en el volcán El Reventador, provincias de Napo y Sucumbíos". URL: https://www.igepn.edu.ec/interactuamos-con-usted/2155-trabajos-de-monitoreo-en-el-volcan-el-reventador-provincias-de-napo-y-sucumbios. Accessed 2025-11-26.

– (2025a). "Informe Volcánico Especial – El Reventador". (2025-001). URL: https://www.igepn.edu.ec/servicios/noticias/2294-informe-volcanico-especial-el-reventador-n-2025-001. Accessed 2025-11-26.

– (2025b). "Informe Volcánico Especial – El Reventador". (2025-002). URL: https://www.igepn.edu.ec/servicios/noticias/2302-informe-volcanico-especial-el-reventador-n-2025-002. Accessed 2025-11-26.

Miwa, T., Y. Iriyama, M. Nagai, and F. Nanayama (2020). "Sedimentation process of ashfall during a Vulcanian eruption as revealed by high-temporal-resolution grain size analysis and high-speed camera imaging". *Progress in Earth and Planetary Science* 7(1). DOI: 10.1186/s40645-019-0316-8.

Miwa, T., N. Geshi, and H. Shinohara (2013). "Temporal variation in volcanic ash texture during a vulcanian eruption at the Sakurajima volcano, Japan". *Journal of Volcanology and Geothermal Research* 260, pages 80–89. DOI: 10.1016/j.jvolgeores.2013.05.010.

Naranjo, M. F., S. K. Ebmeier, S. Vallejo, P. Ramón, P. Mothes, J. Biggs, and F. Herrera (2016). "Mapping and measuring lava volumes from 2002 to 2009 at El Reventador Volcano, Ecuador, from field measurements and satellite remote sensing". *Journal of Applied Volcanology* 5(1). DOI: 10.1186/s13617-016-0048-z.

Pallister, J., R. Wessels, J. Griswold, W. McCausland, N. Kartadinata, H. Gunawan, A. Budianto, and S. Primulyana (2019). "Monitoring, forecasting collapse events, and mapping pyroclastic deposits at Sinabung volcano with satellite imagery". *Journal of Volcanology and Geothermal Research* 382, pages 149–163. DOI: 10.1016/j.jvolgeores.2018.05.012.

Pyle, D. M. (2015). "Sizes of Volcanic Eruptions". *The Encyclopedia of Volcanoes*. Edited by H. Sigurdsson, B. Houghton, S. R. McNutt, H. Rymer, and J. Stix. 2nd edition. Elsevier. Chapter 13, pages 257–264. ISBN: 978-0-12-385938-9. DOI: 10.1016/b978-0-12-385938-9.00013-4.

Valade, S., A. Ley, F. Massimetti, O. D'Hondt, M. Laiolo, D. Coppola, D. Loibl, O. Hellwich, and T. R. Walter (2019). "Towards Global Volcano Monitoring Using Multisensor Sentinel Missions and Artificial Intelligence: The MOUNTS Monitoring System". *Remote Sensing* 11(13), page 1528. DOI: 10.3390/rs11131528.

Vallejo, S., A. K. Diefenbach, H. E. Gaunt, M. Almeida, P. Ramón, F. Naranjo, and K. Kelfoun (2024). "Twenty years of explosive-effusive activity at El Reventador volcano (Ecuador) recorded in its geomorphology". *Frontiers in Earth Science* 11. DOI: 10.3389/feart.2023.1202285.

Vásconez Müller, A., B. Bernard, and F. J. Vasconez (2024). "Near-real-time ash cloud height estimation based on GOES-16 satellite imagery: A case study of the 2022–2023 eruption of Cotopaxi volcano, Ecuador". *Volcanica* 7(1), pages 405–419. DOI: 10.30909/vol.07.01.405419.